

Check for updates

Switching Chirality in Arrays of Shape-Reconfigurable Spindle Microparticles

Mingzhu Liu, Xingyue Han, So Hee Nah, Tianwei Wu, Yuchen Wang, Liang Feng, Liang Wu, and Shu Yang*

The giant circular photo-galvanic effect is realized in chiral metals when illuminated by circularly polarized light. However, the structure itself is not switchable nor is the crystal chirality in the adjacent chiral domains. Here spindle-shaped liquid crystalline elastomer microparticles that can switch from prolate to spherical to oblate reversibly upon heating above the nematic to isotropic transition temperature are synthesized. When arranged in a honeycomb lattice, the continuous shape change of the microparticles leads to lattice reconfiguration, from a right-handed chiral state to an achiral one, then to a left-handed chiral state, without breaking the translational symmetry. Accordingly, the sign of rotation of the polarized light passing through the lattices changes as measured by time-domain terahertz spectroscopy. Further, it can locally alter the chirality in the adjacent domains using near-infrared light illumination. The reconfigurable chiral microarrays will allow us to explore non-trivial symmetry-protected transport modes of topological lattices at the light-matter interface. Specifically, the ability to controllably create chiral states at the boundary of the achiral/chiral domains will lead to rich structures emerging from the interplay of symmetry and topology.

1. Introduction

Artificial lattices that can be reconfigured into a wide range of geometries in nano-/microscales in response to external stimuli will offer dynamically tunable chemical,^[1] mechanical,^[2] optical,^[3] and acoustic properties.^[4] Various approaches and material systems have been developed to achieve pattern transformation. For example, topological transformations of cellular microstructures have been demonstrated by capillarity-induced buckling^[4] or heat-triggered reorientation of liquid crystals (LCs).^[5] Swelling-induced snap-shut of circular pore arrays leads to symmetry breaking of the square array of pores

M. Liu, S. H. Nah, T. Wu, Y. Wang, L. Feng, S. Yang Department of Materials Science and Engineering University of Pennsylvania Philadelphia, PA 19104, USA E-mail: shuyang@seas.upenn.edu X. Han, L. Wu Department of Physics and Astronomy University of Pennsylvania Philadelphia, PA 19104, USA

The ORCID identification number(s) for the author(s) of this article can be found under https://doi.org/10.1002/adma.202303009

DOI: 10.1002/adma.202303009

in hydrogel membranes.^[6,7] More complexity can be achieved by programming the molecular alignment^[2,8-10] or magnetic responsiveness^[11] of the micropillars within an array. Nevertheless, the transformation realized in literature, whether by the closure of the pores, contact of the pillars, or twist of pillars, relies on physically constraining the shape-changing units (pores or pillars) by a stiffer matrix. Thus, the shape change of the individual unit occurs along the *z*-axis, and the residual stress stored in the pores or pillars during fabrication could affect the uniformity of the chirality switch in the microarrays.

The theory has suggested that 2D colloidal crystals assembled from discrete anisometric particles can be reconfigured into different ordered or disordered structures by controlling the shape change of individual particles.^[12,13] Microparticles made from liquid crystal elastomers (LCEs)^[14] can change shapes under various stimuli^[15–17] by programming the molecular director field of LC mesogens

within the microparticle during its formation via surface anchoring^[18] or mechanical shearing.^[19,20] However, continuously changing the shapes of LCE microparticles to different states in a microarray has not been demonstrated. When individual microparticles, especially those with anisotropic shapes, are arbitrarily arranged into microarrays with variable orientations and positions, we expect to generate complex transformation modes, leading to, for example, symmetry breaking from achiral to chiral. When the chiral materials that lack mirror symmetries are illuminated with linearly polarized light, the polarization plane gets rotated, leading to optical activity. [21-23] Symmetry breaking is especially attractive in topological lattices, which host symmetry-protected transport modes where electrons or photons can move only along the edges and surfaces. When photocurrent is selectively switched along the light propagation direction in the terahertz (THz) regime, we could explore potential applications in security, biomedical imaging, wireless communication, and photonic computing.[24-26] Although chiral switches of metamaterials have been reported for THz polarization modulation, [27-29] for example, through deformation of a chiral microelectromechanical system (MEMS) pneumatically, those systems are typically based on hard materials and require large forces to induce deformation. More importantly, it remains challenging to achieve

1521405, 2023, 31, Downloaded from https://onlinelibrary.wiley.com/doi/10.1002/adma.20230090 by University Of Pennsylvania, Wiley Online Library on [29/10/2023], See the Terms and Conditions (https://onlinelibrary.wiley.com/terms-ad-conditions) on Wiley Online Library for rules of use; OA articles are governed by the applicable Creative Commons License

local deformation in currently reported approaches, which will be especially critical to realize topological transitions between the trivial and nontrivial photonic phases.

Here, we synthesize spindle-shaped LCE microparticles with planar surface anchoring using a flow-focusing microfluidic device. After photopolymerization and removal of small molecule LCs, the LC director field within the spherical microdroplets becomes twisted, leading to the formation of spindle-shaped LCE microparticles. Importantly, we show that the shape can be continuously and reversibly reconfigured from prolate to spherical to oblate upon heating to different temperatures. When the spindleshaped microparticles are assembled into a honeycomb lattice with a selected orientation, thus rendering a chiral configuration, the shape change of individual particles induces the transformation of the microarrays from a right-handed chiral state to achiral, then to a left-handed chiral state. By embedding the microarrays in a soft elastomer containing photothermal agents, the transformation of microarrays can be regulated by the near-infrared (NIR) light, enabling spatial control of chirality in the adjacent domains. As a proof-of-concept, we demonstrate that the Faraday rotation angle of light at THz frequencies passing through a chiral microarray can be switched.

2. Results and Discussion

2.1. Synthesis of Spindle-Shaped Microparticles

Spherical microdroplets consisting of non-reactive mesogenic solvent, 4-cyano-4'-pentylbiphenyl (5CB), LC oligomer RM257-1,3 PDT, and LC monomer RM82 in solvent dichloromethane (DCM) are generated via a flow-focusing microfluidic device, [30] suspended in a mixed solution of 5 wt.% poly(vinyl alcohol) (PVA, surfactant, molecular weight 13-23 k) in water, glycerol, and water with a weight ratio of 1:1:2 (Figure 1a,b). 5CB lowers the precursor viscosity while improving surface anchoring strength. Other combinations of oligomers and monomers^[31] can also be used. Then DCM is removed by heating the suspension at a temperature below the nematic to isotropic phase transition temperature (T_{NI}) of the LC mixture, yielding microdroplets with bipolar configuration as PVA promotes planar anchoring at the droplet interface. The resulting microdroplets have diameters in the range of 30–50 µm. The upper limit of 50 µm is limited to the microfluidic device setup, and microdroplets smaller than 30 µm lose the spherical shape after DCM removal and are not polymerizable (Figure S1, Supporting Information). To make bigger microparticles, a microfluidic device with a larger orifice or a more concentrated solution of the precursors in DCM may be used. Considering the penetration depth (≈10 microns) of LC surface anchoring, the diameter of the microparticles should not be too large (on the order of hundreds of microns) using this solventassisted method. Otherwise, the alignment of LC mesogens inside the microdroplets during fabrication could be easily lost. The theoretical lower limit of LCE microparticles is several microns, below which LCs would prefer radial alignments.^[32] Nevertheless, size control is not the focus of this work.

The microdroplets with bipolar configuration are photopolymerized under UV light, changing the director field from bipolar to twisted bipolar as revealed by the change of textures under the polarized optical microscopy (POM), while the shape remains spherical. The change of director field is attributed to anisotropic shrinkage within the particle during polymerization, which is larger at the equator than that at the poles, leading to a larger increase of the splay and bend elastic constants than the twist elastic constant to satisfy the boundary conditions. [33,34] When dispersed in ethanol to extract 5CB, spindle-shaped LCE microparticles are formed (Figure S2, Supporting Information). The photopolymerization temperature is set ≈ 15 °C below the $T_{\rm NI}$ of precursors (65–67 °C) to preserve the director field of the nematic phase, while suppressing the crystallization of monomers at lower temperatures (Figure S3, Table S1, Supporting Information).

The morphology of the microparticles can be tuned by the fraction of 5CB and the molar ratio of oligomers to monomers in the precursors. Well-defined spindle-shaped microparticles are obtained in the range of 30-50 wt.% 5CB (Figure 1c; Figure S4, Supporting Information). Without 5CB, crystallization of the monomers could induce local surface defects, and no shape change is observed after ethanol wash. The shapes of microparticles become non-uniform when the concentration of 5CB is greater than 60 wt.%. By changing the oligomer to monomer molar ratio, we can tune the crosslinking density and T_{NI} of the microparticles (Figure 1d; Figure S5, Supporting Information). POM textures are similar when the molar ratio is in the range of 1.0–1.8; the slightly non-spherical shape is caused by the local variations of the polymerization temperature. When there is no oligomer in the droplet, the polymerized microparticles have the highest crosslinking density and thus show minor shape change after ethanol wash. When the oligomer-to-monomer ratio is increased to 2.5, the network is too soft to support the formation of the spindle shape.

2.2. Reversible Shape Transformation of Microparticles

Upon heated near and beyond $T_{\rm NI}$ (e.g., 180 °C) of the LCEs, the microparticle shrinks along the long axis and expands along the transverse direction continuously, leading to the transformation of the microparticles from prolate to spherical, then to oblate (Figure 2a). A higher oligomer-to-monomer ratio leads to lower LCE crosslinking density, [31] thus lower T_{NI} (Figure 2b). The shape of the microparticles is recovered to the prolate spindle when cooled below T_{NI} (e.g., 60 °C) with slight hysteresis only during the first cycle. The heating and cooling cycles are repeated at least twelve times (Figure 2c,d; Figure S6a, Supporting Information). Birefringence of the microparticles under POM is not completely lost during the heating process (Figure S6b, Supporting Information), suggesting that LC molecules could be partially jammed within the microparticles to resist the phase transition. When heated well-above $T_{
m NI}$ (e.g., 220 °C for a sample with $T_{
m NI}$ of 132 °C), the elastomer network seems to be somewhat disrupted as the particles can only be partially recovered. After the characterization of microparticles' reversible shape transformation behaviors, we now turn our attention to constructing reconfigurable microarrays from them. Such microparticles can also be spatially encoded into an elastomeric film to program its shape morphing from 2D into complex 3D structures.[35]

1521495,2023, 31, Downloaded from https://onlinelibrary.wiley.com/doi/10/1002/dma. 20230909 by University of Pennsylvania, Wiley Online Library on [29/10/2023]. See the Terms and Conditions (https://onlinelibrary.wiley.com/terms-and-conditions) on Wiley Online Library for rules of use; OA articles are governed by the applicable Cerative Commons

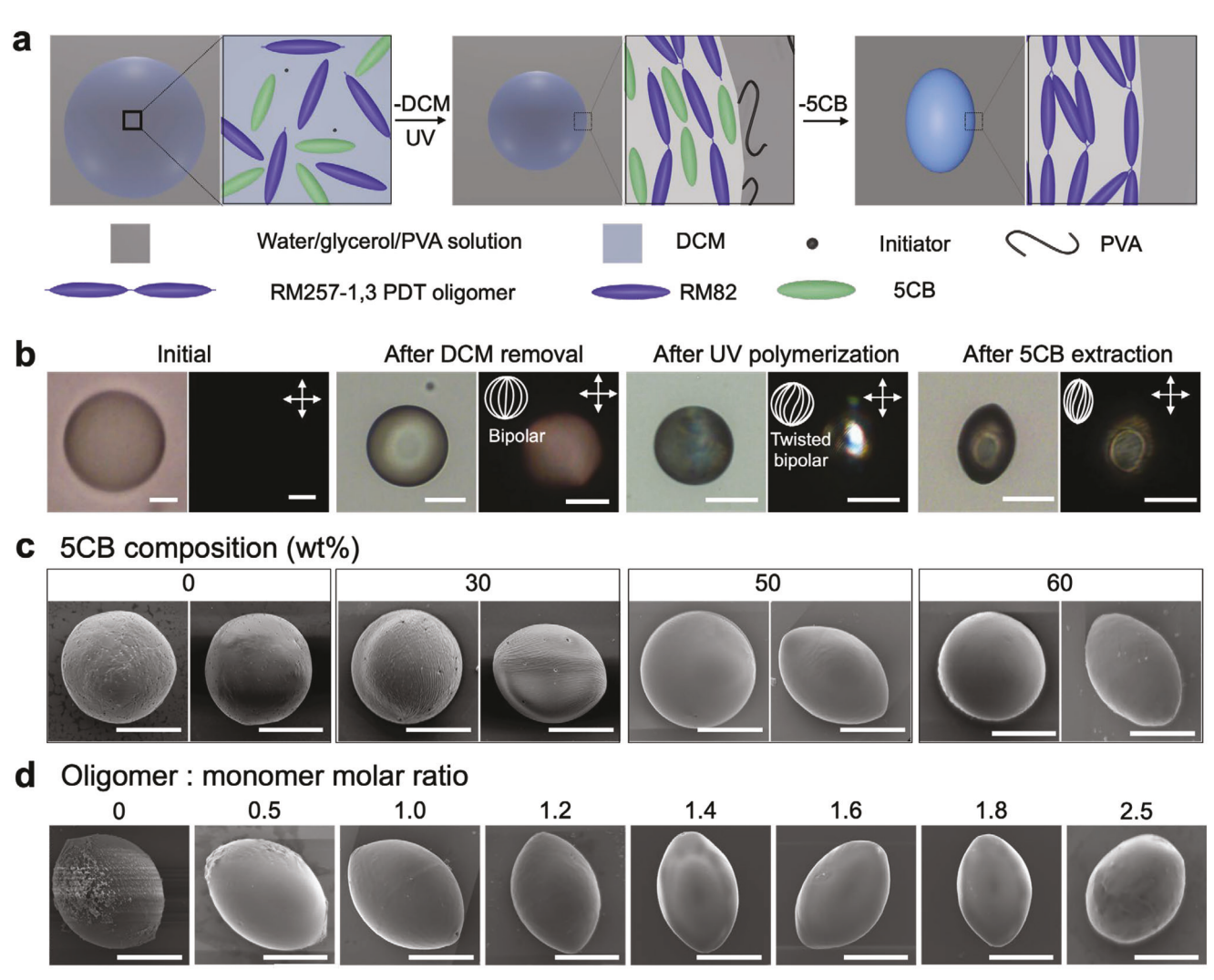


Figure 1. Synthesis of spindle-shaped LCE microparticles. a) Schematic illustrations of the synthesis. b) Bright-field optical microscopy (left) and transmission-mode POM (right) images of the particle at each synthetic step. Inset: the proposed director field. The crossed white double arrows indicate the crossed analyzer and polarizer. c) SEM images of the polymerized microspheres (left) and spindle-shaped microparticles (right) produced after washing with ethanol. Results of different 5CB compositions (0, 30, 50, and 60 wt.%, respectively) are shown. The oligomer-to-monomer molar ratio is kept at 1.4 for all trials. d) SEM images of the spindle-shaped microparticles produced from different oligomer-to-monomer molar ratios. 5CB is kept at 50 wt.% for all trials. Scale bars: 30 μm.

2.3. Packing Microparticles into Microarrays

The top–down fabricated poly(dimethylsiloxane) (PDMS) membranes of oval-shaped holes are used as templates to precisely guide the position and orientation of the microparticles, followed by transferring the microparticles into a soft poly(ethylene glycol) diacrylate (PEGDA) elastomer for the study of thermallyinduced reconfiguration. The length and width of the holes in the PDMS membranes match those of the microparticles (42 and 30 μm , respectively), and the height (20 μm) of the holes is slightly smaller than that of the microparticles (30 μm). Further, the PDMS membranes are rendered hydrophilic by adding poly(dimethylsiloxane-co-ethylene oxide) (PDMS-PEO) in the PDMS precursor to facilitate the microparticle packing and later release from the PDMS template. Microparticles suspended

in ethanol are drop cast onto the PDMS template and dried slowly so that particles can flow into the pre-defined holes driven by capillary force and gravitational force (Figure S7, Supporting Information). The microparticles that are not packed into designated positions are gently squeegeed using a glass slide and blown away. An average of 94.2% \pm 3.8% filling fraction of the microarrays with microparticles in the desired regions (averaged over five randomly selected samples, each has $\approx\!750$ particles) is achieved in the PDMS membranes. To prevent microparticles from rotating out of the holes during their shape change, we transfer the microparticles into a PEGDA thin film (thickness of 200 μ m) to lock their positions (Figure S8, Supporting Information). Since Young's modulus of the microparticles ($\approx\!15.8$ MPa measured from atomic force microscopy, AFM) is 45 times larger than that of the PEGDA ($\approx\!0.35$ MPa measured from the tensile test), the

1521495-2.023, 31, Downloaded from https://onlinelibrary.wiley.com/doi/10/1002/adma.20230909 by University of Pennsylvania, Wiley Online Library on [29/10/2023]. See the Terms and Conditions (https://onlinelibrary.wiley.com/terms-and-conditions) on Wiley Online Library for rules of use; OA articles are governed by the applicable Creative Commons to

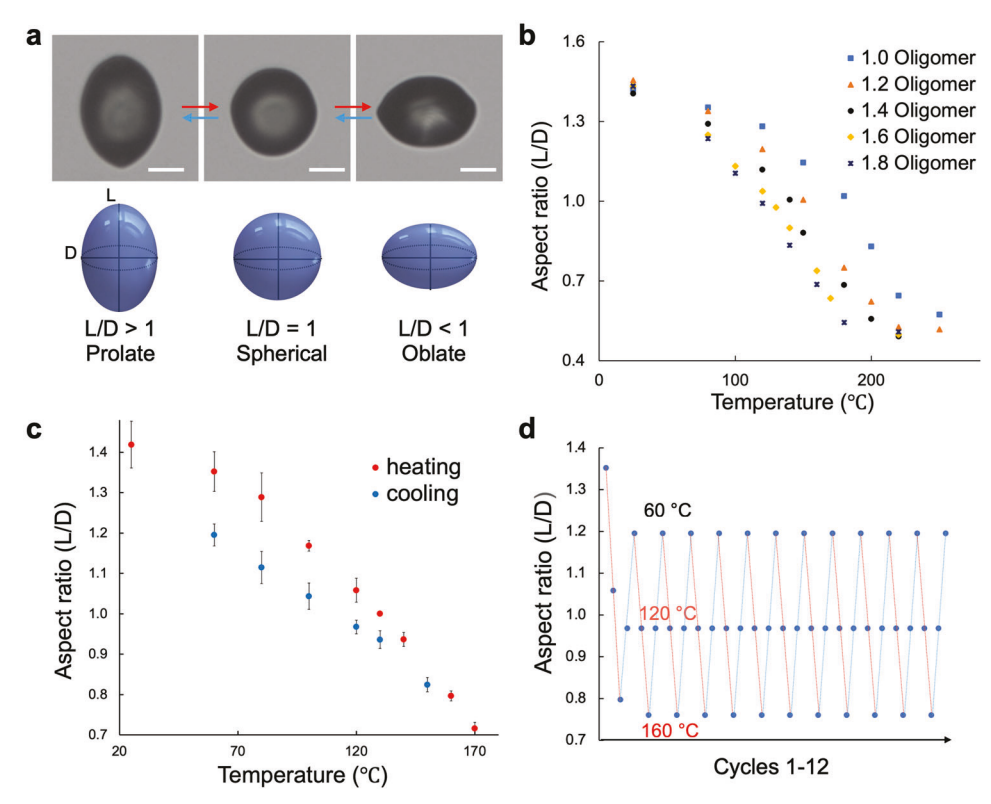


Figure 2. Reversible shape transformation of microparticles. a) Bright-field optical microscopy images and the corresponding schematic illustrations (bottom) of the microparticles during heating and cooling cycles. The shape of the microparticle is defined by the aspect ratio, length along the original long axis (L) over the diameter of the original short axis (D). Scale bars: 20 μm. b) The change of aspect ratio (L/D) of the microparticles versus temperature. c) The change of aspect ratio of the microparticles during the first heating and cooling cycle. The oligomer-to-monomer molar ratio is 1.4. d) The cyclic change of aspect ratios of the microparticles. The oligomer-to-monomer molar ratio is 1.4. The lines are added to guide the eyes: the red lines indicate heating and the blue lines indicate cooling. Each data point in (b–d) is averaged over three randomly picked microparticles. Error bars in (c) represent standard deviations. Standard deviations in (b) and (d) are smaller than 0.05 and therefore they are not shown in the plots.

PEGDA matrix does not interfere with the reversible actuation of the microparticles upon heating and cooling, but keeps them in place.^[35]

2.4. Temperature-Dependent Reconfiguration of Microarrays

Since the shape change of the microparticles is highly dependent on the applied temperature, the chirality of the transformed microarrays is also temperature dependent. As the temperature increases, the microparticles transform from spindle (prolate) at \approx 25 °C to spherical at \approx 140 °C, then to disk-like (oblate) at \approx 180 °C, while their positions are preserved during this process. Comparing the final state with the initial state, the long axes of individual microparticles rotate in-plane synchronously to the transverse direction, which would not have been possible without using microparticles with programmed shape transformation. To take advantage of the anisotropic shape of the microparticles and their "90° rotation" after the shape switch, we arrange them in a honeycomb lattice with the microparticles oriented in a clockwise fashion initially. During the heating and cooling cycles, a reversible switch of the chirality, in the 2D field, from right-handed to achiral, then to left-handed and vice versa is observed, while the threefold translational symmetry is maintained (Figure 3a,b,

Movie S1, Supporting Information). We note that the lattice switches between two different non-symmetric states through a symmetric intermediate state. The birefringence patterns show no noticeable brightness change (Figure S9, Supporting Information), the same as the case of single microparticles. We further demonstrate the transformation of a variety of structures of honeycomb lattices with different spindle orientation angles (90°, 45° , and -45°) and a square lattice following the same procedure (Figure S10, Supporting Information). The shape change of each particle is reversible for at least four cycles (Movie S2, Supporting Information).

As the microparticles are embedded in PEGDA to fix their positions, their shape changes could distort the surrounding matrix, and the particles nearby could compete in such distortions. The degree of the distortion, and correspondingly the transformation temperature, will be highly dependent on Young's modulus contrast between PEGDA and LCE microparticle, the particle packing density, the arrangement, and the interparticle distance. With the same particle density, to realize a certain shape, microparticles placed in an asymmetric chiral pattern require a lower temperature compared with those arranged in a symmetric pattern, where each particle experiences equal competition from all the neighboring particles (Figure S11a, Supporting Information). Intuitively, increasing the interparticle distance can weaken

15214095, 2023, 31, Downloaded from https://onlinelibrary.wiley.com/doi/10.1002/adma.202303009 by University Of Pennsylvania, Wiley Online Library on [29/10/2023]. See the Terms and Conditions (https://onlinelibrary.wiley.com/errns-and-

conditions) on Wiley Online Library for rules of use; OA articles are governed by the applicable Creative Commons

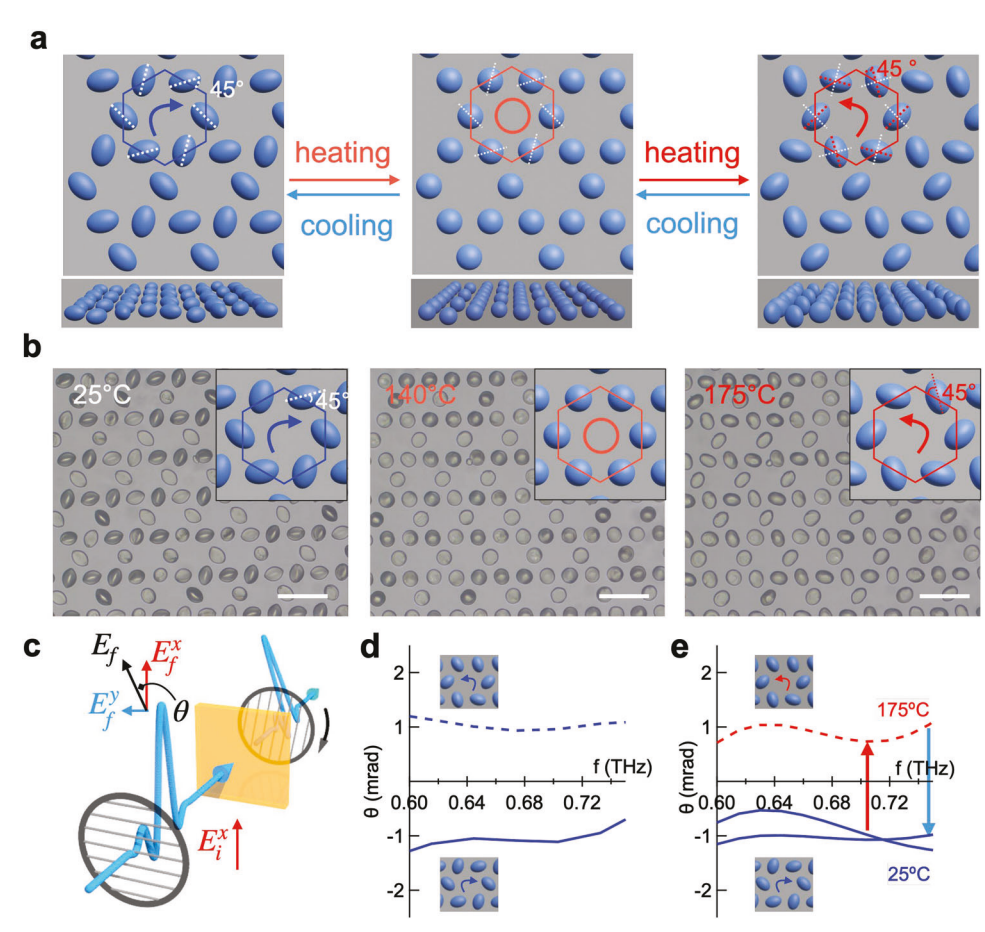


Figure 3. Thermally-induced transformation of honeycomb lattice with chiral configuration. a) Schematic illustrations (top view and side view) of the transformation of the array of microparticles. Each individual particles change shape from prolate to spherical, then to oblate upon heating, leading to the transformation of the chirality of the 2D pattern. The white dashed lines indicate the original arrangement of the microparticles, and the red dashed lines indicate the configurations of the microparticles at elevated temperatures. b) Bright-field optical microscopy images of the honeycomb lattice with the chiral configuration at different temperatures. Inset: scheme of one six-particle unit. Images were taken during the first cycle. Scale bars: $100 \mu m$. c) Schematic illustration of the THz rotation measurement setup. θ is the rotation angle. d) The rotation angles of two samples with different chirality show opposite signs at the initial states. e) The rotation angles of the same sample show the opposite signs at the initial state (25 °C) and the heated state (180 °C).

the competition between particles as the elastomer matrix will dissipate the distortion. As such, the transformation temperature for microparticles in the symmetric patterns decreases when increasing the interparticle distance (Figure S11b, Supporting Information).

2.5. Switchable Circular Birefringence at THz Frequency

Circular birefringence is the rotation of the polarization plane of light after passing through chiral materials. Different chiral metamaterials have distinct chiral resonance frequencies from gigahertz to terahertz. We use a time-domain THz spectroscopy (Figure 3c) to measure the rotation of the polarization plane of light passing through the microarrays before and after heating. The incident THz radiation is vertically polarized (E_i^x) using a wire grid polarizer. The transmitted THz radiation (E_f) has a polarization plane at an angle θ from the vertical plane

(referred to as the THz rotation angle). The vertical (E_c^x) and horizontal (E_{ϵ}^{γ}) projections of E_{ϵ} are analyzed by a second polarizer mounted on the rotation stage.[39] As a first test, we measure two samples with an opposite chirality at room temperature, and they show opposite signs of θ at initial states before heating (Figure 3d). The solid line represents the clockwise sample which produces negative rotation values, and the dashed line represents the counterclockwise sample with positive values. Both have an amplitude ≈1 mrad from 0.6 to 0.75 THz (The broader frequency dependence is shown in Figure S12, Supporting Information). Next, we perform reversible switching by heating and measuring the THz rotation. As shown in Figure 3e, the chirality switching of the microarray overthe heating and cooling cycle results in significant changes of θ . Heating the clockwise sample from 25 to 175 °C reverses the sign of θ , consistent with the counterclockwise pattern at 175 °C (Figure 3e, red arrow). The sign of θ recovers after being cooled to 25 °C, indicating the reversibility of the



15214095, 2023, 31, Downloaded from https://onlinelibrary.wiley.com/doi/10.1002/adma_20230909 by. University of Pennsylvania, Wiley Online Library on [29/10/2023]. See the Terms and Conditions (https://onlinelibrary.wiley.com/erms-and-conditions) on Wiley Online Library for rules of use, OA articles as a governed by the applicable Cerative Commons

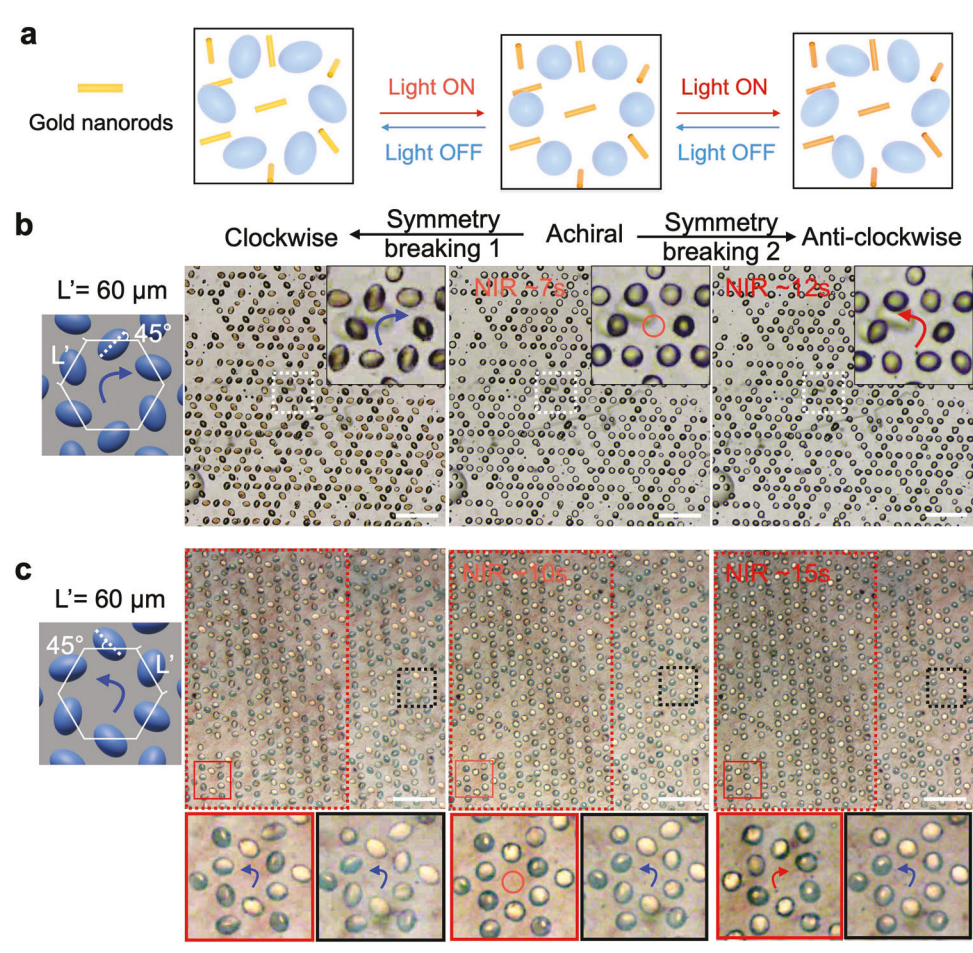


Figure 4. NIR light-induced chirality transformation. a) Schematic illustrations of the transformation of one lattice unit under NIR light illumination. b) Bright-field optical microscopy images of the honeycomb lattice under NIR light illumination, demonstrating chirality change. Initially, the LCE spindles are packed in a clockwise configuration and embedded in PEGDA with gold nanorods. NIR light intensity: 3 W cm⁻². c) Bright-field optical microscopy images of the pattern transformation when only the left part (inside of the red dotted box) is illuminated by NIR laser through a photomask. Bottom: Enlarged images showing the selected regions that undergo the chirality switch (red boxes) or maintain the original chirality (black boxes). Scale bars: 200 μm.

transformation of microarrays (Figure 3e, blue arrow). To further validate the origin of the optical activity as the result of the chirality switch of the microarrays, we perform a 3D full wave simulation (Figure S13, Supporting Information). The simulation results qualitatively agree with the experimental measurements, show opposite signs of θ when the THz light passes through the microarrays of different chirality, but no rotation when there is no microparticles.

2.6. Light-Triggerable Spatially Programmable Transformation of Microarrays

It will be intriguing to realize multiple topological transitions between the trivial and nontrivial photonic phases by locally reconfiguring the orientation of the lattice units without altering their global geometry. Therefore, through the combination of the topologically protected edge states and reconfigurable topological one-way propagation of the "non-trivial" states, we could freely steer light propagations in a 2D or 3D space. Such kind of reconfigurable topological switches has been explored theoretically in the microwave frequency from 2D dielectric photonic crystals in a triangular lattice of elliptical cylinders. [40,41] Here, to attest the possibility of local switching of chirality, 0.1 wt.% gold nanorods (Figure 4a; Figure S14, Supporting Information) are added to the PEGDA precursor as the photothermal agents that can convert NIR light into heat. [42] This way, we can use light to heat the matrix both globally and locally. The microarray first undergoes a global transformation when the entire sample is exposed to the 808 nm laser beam (reaching ≈170–180 °C after 12 s exposure with an intensity of ≈ 3 W cm⁻², Figure 4b). Similar to the effect of using the hot stage, two distinct chiral states can be produced through the symmetry breaking of an intermediate symmetric structure. The transformation using the NIR light is much faster (several seconds) compared to heating on a hot plate (several minutes) and recovers instantly when the NIR light is off (Movie S3, Supporting Information). The brightness of birefringence under POM is not lost during the shape-changing process under NIR light (Figure S15, Supporting Information).

www.advancedsciencenews.com

ADVANCED MATERIALS

www.advmat.de

15214055, 2023, 31, Downloaded from https://onlinelibrary.wiley.com/doi/10/1002/dma. 20230090 by. University of Pennsylvania, Wiley Online Library on [29/10/2023]. See the Terms and Conditions (https://onlinelibrary.wiley.com/terms-and-conditions) on Wiley Online Library for rules of use; OA articles are governed by the applicable Cerative Commons

We then expose the sample to a NIR laser through a photomask (see the setup in Figure S16, Supporting Information) so that the microarray can be locally transformed. The exposed region undergoes the transformation from anti-clockwise to clockwise while the other parts remain anti-clockwise (Figure 4c, Movie S4, Supporting Information). The slight shape change in the blocked edges can be attributed to the heat transfer from the exposed region to the blocked region. Such designable, spatially controlled transformation via local heating through the photothermal effect of the gold nanorods will offer a new pathway to regulate polarization in THz in 2D space. We note careful selection of the local heating materials that do not interfere with the optical activities enabled by the transforming microparticle arrays in THz will be important.

3. Conclusion and Outlook

In summary, we create LCE microparticles that can undergo reversible and substantial shape changes upon heating and cooling. When the microparticles are packed into arrays, the transformation of individual particles induced by heating or NIR light illumination leads to the change of chirality of the microstructures without breaking the translational symmetry, which is confirmed by the reversal of the Faraday rotation angle of THz light. The optical response obtained from our system is relatively small compared with the values reported in the literature. [27–29] We believe this could be further improved by optimization of the component materials, design of microarray geometries, assembly of multiple layered microparticle arrays for switching from 2D to 3D, and introduction of gradient assembly of microparticles. Nevertheless, our system is unique in terms of its ability to dynamically and locally control the chirality switch, which would otherwise be challenging to achieve in existing metamaterial systems. [27] The freely reconfigurable microarrays produced from our approach overcome the deformation limitations in MEMS and the rigid substrate effect of soft lattices in a continuous medium, which will allow for non-reciprocal motions in lattices with non-collinear symmetry axes, [9] or actuations on curved surfaces. As the pattern design is decoupled from the syntheses of the building blocks, more complex patterns and programmable transformations can be realized for potential applications including topological photonic switches, dynamic waveguiding, adaptive surfaces, and reconfigurable optoelectronic devices.

4. Experimental Section

Synthesis of RM257-13PDT Oligomers: The oligomers (RM257-1,3 PDT) were synthesized following a reported procedure. [31] In detail, 10.0 g of 1,4-bis-[4-(3-acryloyloxy-proplyoxy)benzoyloxy]-2-methylbenzene (RM257, >95%, Wilshire Technologies Inc.) and 3.68 g 1,3-propanedithiol (1,3 PDT, >99%, Sigma-Aldrich) were added into a 250 mL round-bottom flask. Then 100 mL dichloromethane (DCM, Fisher Scientific) was added to dissolve these chemicals with a stirring speed at 400 rpm, yielding a transparent solution. After that, four drops (≈0.2 mL) of 1,8-diazabicyclo(5.4.0) undec-7-ene (DBU, Sigma-Aldrich) were added as the catalyst and the solution was stirred at room temperature (≈25 °C) for 24 h. The mixture was washed with hydrochloric acid (HCl, 37%, Sigma-Aldrich) aqueous solution twice (first 1 m then 0.1 m, saturated sodium chloride (NaCl, Sigma-Aldrich) was used to enhance the separation of

the organic phase and the aqueous phase). The DCM solution was then dried by magnesium sulfate (MgSO $_4$, anhydrous powder, Fisher Scientific) for 30 min and filtrated to remove MgSO $_4$. Finally, 20 mg (0.2 wt.% of RM257) butylated hydroxytoluene (BHT, Sigma-Aldrich) was added into the LC oligomer solution and the oligomers were collected as a viscous liquid after evaporating the DMC by RV 8 FLEX rotary evaporator. The viscous liquid was collected in a vial and stored in the freezer (the transparent liquid turned opaque white after two days in a freezer). Experiments were carried out in a lab equipped with yellow light.

Synthesis of Gold Nanorods (AuNRs) and Surface Modification: AuNRs were synthesized by following a standard seed-mediated method. [42] In a typical procedure, a seed solution was first prepared by adding 0.25 mL $0.01~{\rm M~HAuCl_4\cdot 3H_2O}$ (Sigma-Aldrich) to 9.75 mL 0.10 M CTAB (Sigma-Aldrich) aqueous solution in a 20 mL scintillation vial. Then, 0.60 mL of freshly made 0.01 M NaBH₄ aqueous solution was quickly injected into the mixed solution of HAuCl₄·3H₂O and CTAB under vigorous stirring. The color of the solution turned brownish-yellow, and the stirring was stopped after 2 min. The seed solution was aged at room temperature for 30 min before further usage. To prepare the growth solution, 10 mL 0.01 M HAuCl₄·3H₂O and 1.5 mL 0.01 M AgNO₃ (≥99%, Sigma-Aldrich) were added to 237.5 mL 0.10 M CTAB in a 250 mL flask. The solution was slowly stirred for 15 min followed by adding 1.6 mL 0.1 M ascorbic acid (BioUltra, ≥99.5%, Sigma-Aldrich). Finally, 1.8 mL seed solution was added to the mixture. The solution was gently mixed and left at 30 °C for at least 3 h. The AuNRs solution was centrifuged at 9000 rpm for 20 min (Eppendorf centrifuge 5804R) twice to remove excess CTAB and added into 20 mL $2\,\mathrm{mm}$ PEG-SH ($800\,\mathrm{g}\,\mathrm{mol}^{-1}$, Sigma-Aldrich) solution, sonicated, and sat still for 24 h. The AuNRs solution was centrifugated at 8500 rpm for 20 min and the supernatant was decanted. Finally, the AuNRs were dispersed in the ethanol.

Microfluidic Device for Microdroplets Fabrication: A flow-focusing microcapillary device^[30] was assembled for the fabrication of microdroplets. The diameter of the orifice of the inner capillary was ≈200 µm. The aqueous phase was 1:1 wt:wt glycerol: 5% PVA (13-23k), and the outer phase was a precursor solution of 5CB, RM 82, oligomer (RM257-1,3-PDT), and initiator DMPA dissolved in DCM (0.25 g mL⁻¹). The ratios of monomer and oligomer could be varied (Table S1, Supporting Information). The $T_{\rm NL}$ of the mixture was measured by drop casting 20 µL of the DCM solution onto a glass slide and observing the texture change with temperature under POM after the DCM was evaporated (overnight in the fume hood at 25 °C room temperature). The aqueous phase and organic phase were filtered through PES and PTFE membrane filters with 0.22 µm cut-off pore size before usage, respectively. Microdroplets were collected in a vial with a mixture of 5 mL 1:1 wt:wt Glycerol: 5% PVA (13-23 k) and 5 mL water (10 mL of 1.25 wt.% PVA and 25 wt.% glycerol in water). Typical fabrication speeds were 300 μ L h⁻¹ for the inner phase and 2400 μ L h⁻¹ for the outer phase. The size of the microdroplets was tuned by the concentration of the precursors in DCM. A concentration of 0.25 g mL⁻¹ was usually used to target 50 µm (diameter) particles by producing 80 µm microdroplets in the microfluidic device. This solution was diluted with DCM to target smaller sizes. For example, 200 μL of the solution (0.25 g $mL^{-1})$ was diluted to 1 mL (0.05 g mL $^{-1})$ to make final microparticles of 30 μm (diameter) from the same-sized 80 µm DCM precursor microdroplets.

Synthesis of LCE Microparticles: The 20 mL vial, with microdroplets (consisting of 5CB, and LC oligomers and monomers as the LCEs precursor in DCM) suspended in a mixed solution of 1.25 wt.% PVA and 25 wt.% glycerol in water, was placed on the heating plate with the cap opened at 50 °C overnight. The vial was gently shaked every several hours to promote the evaporation of DCM and prevented particles from sticking onto the bottom surface of the vial. Stirring might break apart the droplets, therefore, they were not stirred during heating. To study the impact of temperature, hot plates with different temperatures were used, including 2 days at room temperature, 8 h at 35 °C, 6 h at 50 °C, or 4 h at 65 °C. This duration could be prolonged to ensure the complete removal of DCM. The vials were shaken to make sure no particles stuck to the bottom of the vials before UV polymerization to prevent nonuniform particle production. After DCM removal, the vial was capped (on the heating plate) and exposed to UV light (365 nm, \approx 20 mW cm $^{-2}$, DC4104 4-channel LED, Thorlabs) for

1521495-2.023, 31, Downloaded from https://onlinelibrary.wiley.com/doi/10/1002/adma.20230909 by University of Pennsylvania, Wiley Online Library on [29/10/2023]. See the Terms and Conditions (https://onlinelibrary.wiley.com/terms-and-conditions) on Wiley Online Library for rules of use; OA articles are governed by the applicable Creative Commons to

1 h, during which the vial was gently shaken about every 10 min to prevent the particles from sediment. After polymerization, particles were allowed to sediment and concentrate (\approx 30 min) before washing with DI water or ethanol (overnight) three times, respectively.

Observation of the Reversible Shape Reconfiguration of Single Microparticles: Glass substrates were precleaned by rinsing with acetone three times, followed by drying with an air gun. Several microliters of spindle-shaped microparticles dispersed in ethanol were drop casted and dried onto a glassy slide. This slide was then put into a thermal stage (Linkam Scientific Instruments Ltd., LTS420) equipped with the optical microscope (Zeiss, axio imager.M2m) to study the shape change upon heating and cooling cycles. The heating speed was set to 10 °C min⁻¹, and the sample was held at a certain temperature for 1 min before capturing images. The shape change during this holding time was minimal.

Fabrication of PDMS Templates: Photomasks were prepared by direct writing the patterns on the soda lime glass substrates (photoresist AZ1500) using the Heidelberg DWL 66+ Laser Writer, followed by developing in Microposit MF-319 (Kayaku Advanced Materials), etching by Chrome Etch 1020AC (Transene Inc.), and stripping in Microposit Remover 1165 (Kayaku Advanced Materials), respectively. Photomasks for NIR light exposure were fabricated in the same way. To create a master, OmniCoat (Kayaku Advanced Materials) and 20 µm of SU-8 2025 (Kayaku Advanced Materials) were spin-coated onto the Si wafer sequentially. The wafer was exposed to UV light (365 nm, 130 mJ cm⁻²) with the photomask aligner (SUSS MicroTec MA6 Gen3 Mask Aligner). Then the wafer was developed in SU-8 developer (Kayaku Advanced Materials) to obtain ovalshaped pillars with a height of 20 µm. Poly(dimethylsiloxane-co-ethylene oxide) (PDMS-PEO, Polysciences Inc.) was added to the PDMS base and curing agent (Sylgards 184 Silicone elastomer kit, Dow Corning) in 1:5:50 by weight. The PDMS mixture was poured onto the wafer and cured at 65 °C for 2 h. The fully cured PDMS-PEO template was peeled off from the silicon wafer with oval-shaped holes that LCE particles could settle in. The PEO component made the template hydrophilic, which both promoted the particle packing and facilitated the later transferring process.

Assembly of LCE Microparticles in PDMS Template: The suspension of microparticles in ethanol ($\approx\!1\%$ wt/v, weight of microparticles in mg over volume of ethanol in $\mu L)$ was shaken before dispensing 40 μL onto the PDMS template. The PDMS substrate was left inside a petri dish with a cover and allowed to dry for $\approx\!4$ h. The sample was checked under an optical microscope to confirm the packing of microparticles guided by the pattern. Microparticles not trapped in the templated holes could be removed by carefully squeegeeing the PDMS surface with a glass slide and blowing away with a compressed air duster (Falcon Dust, Off Compressed Gas (152a) Disposable Cleaning Duster). This process could be repeated to improve the packing fraction.

Transferring Microarrays into Elastomer: Elastomer precursor was prepared by mixing poly(ethylene glycol) diacrylate (PEGDA, 2.8 g, average Mn 700, Sigma-Aldrich), 2,2'-(Ethylenedioxy)diethanethiol (EDDT, 1.28 g, 95%, Sigma-Aldrich), pentaerythritol tetrakis (3mercaptopropionate) (PETMP, 0.36 g, >95%, Sigma-Aldrich), 2-Hydroxy-2-methylpropiophenone (Darocur 1173, 42 mg, Sigma-Aldrich, 1.5 wt.% based on PEGDA, photoinitiator), and methylhydroquinone (MEHQ, 56 mg, Sigma-Aldrich, 2 wt.% based on PEGDA, inhibitor). About 10 μL precursor was cast onto a clean glass (2.5 cm × 2.5 cm watch glass, Fisher Scientific, blown with compressed air before usage) with a 100-µm-thick PDMS spacer. Then the PDMS pattern with microparticles was applied onto the drop and allowed the precursor to diffuse for 5 min before UV exposure (200 mW cm⁻²) for 5 min. The glass with elastomer-embedded microparticles was carefully peeled off the PDMS pattern. Then another 100-μm-thick PDMS spacer was used to cover the top of the sample with PEGDA elastomer. This precursor mixture should be prepared within one week of usage to avoid the effect of gelation. For the samples used for NIR light-induced reconfiguration, 0.1 wt.% gold nanorods were added into the elastomer precursor.

Observation of the Pattern Transformation: The elastomer with embedded microarrays of microparticles was put onto a glass slide. Then the sample was heated/cooled inside a thermal chamber at the speed of $20~^{\circ}\text{C}$ min $^{-1}$. For light-induced transformation, the sample was put un-

der a microscope, and a NIR laser (808 nm, \approx 3 W cm $^{-2}$) was turned on from a portable infrared laser pointer (LaserTo). Images were captured at selected temperatures or different light exposure durations. Videos were taken at the same setup.

Measurement of Polarization Rotation in Microarrays: A time-domain terahertz (THz) spectroscopy was used to measure the circular birefringence of the chiral microarrays. A fiber laser (780 nm, 82 fs, Toptica, FemtoFiber smart 780) was split into pump and probe beams. The pump beam excited a photoconductive antenna to emit THz radiation. The copropagating THz signal and the probe beam overlapped at the THz detector (another photoconductive antenna). The retardation between the two beams was controlled by a delay stage to measure the entire time profile of the THz electric field signal. The frequency-domain signal was then extracted with Fourier transformations. The polarization rotation was computed from $\theta = E_f^{\gamma}(\omega)/E_f^{x}(\omega)$. The temperature of the microarray sample was controlled by a hot plate (Thermo Scientific Cimarec SP88854105).

Simulation: 3D full wave simulations based on finite element methods were used to simulate the transmission with a vertical incidence. Figure S13 (Supporting Information) shows the details of the setup. Refractive indices of 3.0 and 1.3 were used for microparticles and matrix, respectively. The polarization rotation angle $\Delta\alpha$ of a linear-polarized light was calculated by $\Delta\alpha=(\varphi_R-\varphi_L)/2$.

Characterization: Bright-field microscopy images, videos, and POM images were obtained using an Olympus BX61 Motorized Microscope equipped with crossed polarizers. Bright-field microscopy images during heating and cooling cycles were taken with a Zeiss microscope (Axio imager.M2m) equipped with a thermal stage (Linkam Scientific Instruments Ltd., LTS420). SEM images of particles were taken from an FEI Quanta 600 environmental scanning electron microscopy at a 3 kV electron beam. Particles were dried on a silicon wafer and sputter coated with Iridium (Ir) with a thickness of 4 nm before imaging. Some images were digitally post-processed to improve brightness and contrast. Transmission electron microscopy image of gold nanorods was taken on a JEOL JEM-F200 at 200 kV. Absorbance spectra of gold nanorods were collected from the Agilent Cary 5000 UV-vis-NIR spectrophotometer from 400 to 1000 nm with an interval of 1 nm and scanning rate of 600 nm min⁻¹.

Supporting Information

Supporting Information is available from the Wiley Online Library or from the author.

Acknowledgements

The authors acknowledge Professor Daeyeon Lee for access to the instruments to prepare the microfluidic devices. Dr. Jiagi Liu, Dr. Lishuai Jin, and Professor Andrej Košmrlj (Princeton University) are acknowledged for their helpful discussions. This work was supported in part by National Science Foundation (NSF) through the Materials Research Science and Engineering Center (MRSEC) at the University of Pennsylvania (DMR-1720530, to S.Y.and L. W.) and DMR/Polymer program (DMR-2104841, to S.Y). This work utilized the facilities at the Singh Center for Nanotechnology, which was supported by the NSF National Nanotechnology Coordinated Infrastructure Program under Grant No. NNCI-2025608. The development of the THz polarity measurement was supported by the Army Research Office (ARO)/YIP award (to L.W.) under Grant No. W911NF1910342. X.H. was partially supported by the Gordon and Betty Moore Foundation's EPiQS Initiative Grant No. GBMF9212 to L.W. L.W. also acknowledges partial summer support from the NSF/EArly-concept Grants for Exploratory Research (EAGER) grant (Grant No. DMR2132591).

Conflict of Interest

The authors declare no conflict of interest.

Author Contributions

M.L., L.W., and S.Y. conceived the idea; M.L. led the experiments and prepared the samples; S.N. fabricated the PDMS templates; X.H. carried the THz measurements; T.W. performed the simulation under L.F.'s supervision. Y.W. synthesized the gold nanorods; M.L., X.H., S.N., Y.W., L.W., and S.Y. wrote the manuscript; all authors discussed the results and reviewed the manuscript.

Data Availability Statement

The data that support the findings of this study are available in the supplementary material of this article.

Keywords

liquid crystalline elastomers, optical rotation, reconfigurable microarrays, switchable chirality, symmetry breaking

Received: April 1, 2023 Revised: May 29, 2023 Published online: June 5, 2023

- [1] L. D. Zarzar, J. Aizenberg, Acc. Chem. Res. 2014, 47, 530.
- [2] J. Cui, D. M. Drotlef, I. Larraza, J. P. Fernandez-Blazquez, L. F. Boesel, C. Ohm, M. Mezger, R. Zentel, A. Del Campo, Adv. Mater. 2012, 24, 4601.
- [3] J. Ma, C. Ouyang, L. Niu, Q. Wang, J. Zhao, Y. Liu, L. Liu, Q. Xu, Y. Li, J. Gu, Z. Tian, J. Han, W. Zhang, Opt. Express 2021, 29, 32105.
- [4] S. Li, B. Deng, A. Grinthal, A. Schneider-Yamamura, J. Kang, R. S. Martens, C. T. Zhang, J. Li, S. Yu, K. Bertoldi, J. Aizenberg, *Nature* 2021, 592, 386.
- [5] S. Li, G. Librandi, Y. Yao, A. J. Richard, A. Schneider-Yamamura, J. Aizenberg, K. Bertoldi, Adv. Mater. 2021, 33, 2105024.
- [6] G. Wu, Y. Xia, S. Yang, Soft Matter 2014, 10, 1392.
- [7] B. Cao, G. Wu, Y. Xia, S. Yang, Extreme Mech. Lett. 2016, 7, 49.
- [8] Y. Yao, J. T. Waters, A. V. Shneidman, J. Cui, X. Wang, N. K. Mandsberg, S. Li, A. C. Balazs, J. Aizenberg, Proc. Natl. Acad. Sci. U. S. A 2018, 115, 12950
- [9] S. Li, M. M. Lerch, J. T. Waters, B. Deng, R. S. Martens, Y. Yao, D. Y. Kim, K. Bertoldi, A. Grinthal, A. C. Balazs, J. Aizenberg, *Nature* 2022, 605, 76.
- [10] J. T. Waters, S. Li, Y. Yao, M. M. Lerch, M. Aizenberg, J. Aizenberg, A. C. Balazs, Sci. Adv. 2020, 6, eaay5349.
- [11] J. E. Park, J. Jeon, S. J. Park, S. Won, Z. Ku, J. J. Wie, ACS Nano 2022, 16, 18101.
- [12] T. D. Nguyen, E. Jankowski, S. C. Glotzer, ACS Nano 2011, 5, 8892.
- [13] N. Tanjeem, M. B. Minnis, R. C. Hayward, C. W. T. Shields, Adv. Mater. 2021, 34, 2105758.
- [14] S. W. Ula, N. A. Traugutt, R. H. Volpe, R. R. Patel, K. Yu, C. M. Yakacki, Liq. Cryst. Rev. 2018, 6, 78.

- [15] J. Q. Liu, Y. C. Gao, Y. J. Lee, S. Yang, Trends Chem. 2020, 2, 107.
- [16] L. B. Braun, T. Hessberger, R. Zentel, J. Mater. Chem. C 2016, 4, 8670.
- [17] X. Liu, R. Wei, P. T. Hoang, X. Wang, T. Liu, P. Keller, Adv. Funct. Mater. 2015, 25, 3022.
- [18] T. Lopez-Leon, A. Fernandez-Nieves, Colloid Polym. Sci. 2011, 289, 345.
- [19] X. Liu, X. Pan, M. G. Debije, J. P. A. Heuts, D. J. Mulder, A. Schenning, Soft Matter 2020, 16, 4908.
- [20] C. Ohm, N. Kapernaum, D. Nonnenmacher, F. Giesselmann, C. Serra, R. Zentel, J. Am. Chem. Soc. 2011, 133, 5305.
- [21] Z. Ni, K. Wang, Y. Zhang, O. Pozo, B. Xu, X. Han, K. Manna, J. Paglione, C. Felser, A. G. Grushin, F. De Juan, E. J. Mele, L. Wu, *Nat. Commun.* 2021, 12, 154.
- [22] Z. Ni, B. Xu, M. A. Sanchez-Martinez, Y. Zhang, K. Manna, C. Bernhard, J. W. F. Venderbos, F. De Juan, C. Felser, A. G. Grushin, L. Wu, npj Quantum Mater. 2020, 5, 96.
- [23] M. Funahashi, Y. Mori, Mater. Chem. Front. 2020, 4, 2137.
- [24] L. S. Madsen, F. Laudenbach, M. F. Askarani, F. Rortais, T. Vincent, J. F. F. Bulmer, F. M. Miatto, L. Neuhaus, L. G. Helt, M. J. Collins, A. E. Lita, T. Gerrits, S. W. Nam, V. D. Vaidya, M. Menotti, I. Dhand, Z. Vernon, N. Quesada, J. Lavoie, *Nature* 2022, 606, 75.
- [25] J. Wang, S. Xia, R. Wang, R. Ma, Y. Lu, X. Zhang, D. Song, Q. Wu, R. Morandotti, J. Xu, Z. Chen, Light Sci. Appl. 2022, 11, 152.
- [26] T. Nagatsuma, G. Ducournau, C. C. Renaud, Nat. Photonics 2016, 10, 371
- [27] T. Kan, A. Isozaki, N. Kanda, N. Nemoto, K. Konishi, H. Takahashi, M. Kuwata-Gonokami, K. Matsumoto, I. Shimoyama, *Nat. Commun.* 2015, 6, 8422
- [28] S. Zhang, J. F. Zhou, Y. S. Park, J. Rho, R. Singh, S. Nam, A. K. Azad, H. T. Chen, X. B. Yin, A. J. Taylor, X. Zhang, *Nat. Commun.* 2012, 3, 942.
- [29] N. Kanda, K. Konishi, M. Kuwata-Gonokami, Opt. Lett. 2014, 39,
- [30] A. S. Utada, L. Y. Chu, A. Fernandez-Nieves, D. R. Link, C. Holtze, D. A. Weitz, MRS Bull. 2011, 32, 702.
- [31] Y. Xia, X. Zhang, S. Yang, Angew. Chem., Int. Ed. 2018, 57, 5665.
- [32] D. S. Miller, X. Wang, N. L. Abbott, Chem. Mater. 2014, 26, 496.
- [33] H. S. Ansell, D. S. Kim, R. D. Kamien, E. Katifori, T. Lopez-Leon, Phys. Rev. Lett. 2019, 123, 157801.
- [34] X. Wang, E. Bukusoglu, D. S. Miller, M. A. Bedolla Pantoja, J. Xiang, O. D. Lavrentovich, N. L. Abbott, Adv. Funct. Mater. 2016, 26, 7343.
- [35] M. Liu, L. Jin, S. Yang, Y. Wang, C. B. Murray, S. Yang, Adv. Mater. 2023. 35, 2208613.
- [36] S. Yang, Y. Li, X. Chen, Q. Yang, J. Han, W. Zhang, Opt. Lett. 2020, 45, 6146.
- [37] S. Lee, S. Baek, T. T. Kim, H. Cho, S. Lee, J. H. Kang, B. Min, Adv. Mater. 2020. 32. 2000250.
- [38] D. L. Sounas, C. Caloz, A. Alu, Nat. Commun. 2013, 4, 2407.
- [39] X. Han, A. Markou, J. Stensberg, Y. Sun, C. Felser, L. Wu, *Phys. Rev. B* 2022, 105, 174406.
- [40] H. B. Huang, S. Y. Huo, J. J. Chen, Crystals 2019, 9, 221.
- [41] J. Chen, H. Huang, S. Huo, Z. Tan, X. Xie, J. Cheng, G.-L. Huang, Phys. Rev. B 2018, 98, 014302.
- [42] Y. Wang, A. Dang, Z. Zhang, R. Yin, Y. Gao, L. Feng, S. Yang, Adv. Mater. 2020, 32, 2004270.